IEEE Transactions on Components and Packaging Technologies

The Relationship between Contact Resistance and Contact Force on Au coated Carbon Nanotube surfaces under Low Force Conditions.

Journal:	*IEEE Transactions on Components and Packaging Technologies*
Manuscript ID:	TCPT-2008-066
Manuscript Type:	Electrical Contacts
Date Submitted by the Author:	17-Apr-2008
Complete List of Authors:	McBride, John; University of Southampton, School of Engineering Sciences Yunus, Esa; Univesrity of Southampton, School of Engineering Sciences Spearing, Simon; Univesrity of Southampton, School of Engineering Sciences; Univesrity of Southampton, School of Engineering Scinces
Keywords:	nano-indentation apparatus, Contact resistance, carbon nanotubes, Au/multi walled carbon nanotubes

The Relationship between Contact Resistance and Contact Force on Au coated Carbon Nanotube surfaces under Low Force Conditions.

E. M. Yunus pgesa@soton.ac.uk
J.W. McBride J.W.Mcbride@soton.ac.uk
S.M Spearing Spearing@soton.ac.uk
School of Engineering Sciences, University of Southampton SO17 1BJ

***Abstract*-Carbon-Nanotube (CNT) coated surfaces are investigated to determine the electrical contact performance under low force conditions. The surfaces under investigation are vertically aligned multi-walled CNTs formed on a Silicon substrate and coated with an Au film. These planar surfaces are mated with a hemispherical Au plated probe mounted in a nano-indentation apparatus. The maximum contact force used is 1mN. The contact resistance of these surfaces is investigated as a function of the applied force and is also studied under repeated loading cycles. The surfaces are compared with a reference Au-Au contact under the same experimental conditions and the results compared to established contact theory. The results show that the vertically aligned multi-walled CNT surface provides a stable contact resistance. This study shows the potential for the application of CNT surfaces as an interface in low force electrical contact applications.**

Keywords: nano-indentation apparatus, contact resistance, carbon nanotubes, and Au/multi walled carbon nanotubes.

I. INTRODUCTION.

This paper presents a study of electrical contact surfaces under low force conditions, typically below 1mN. Such conditions are relevant to micro-contact applications, for example MEMS relay devices. There are a number of potential contact materials for such applications; Gold, Palladium or Platinum are commonly used [1]. The main disadvantage of these materials is that they are relatively soft and easily wear. Other potential contact materials for the low force applications are silicon carbide and diamond, however both have high elastic moduli coupled with low electrical conductivity. SiC film doped with NH_3 has a resistivity of to 1 x 10^{-4} Ωm [2] and DLC (Diamond Like Carbon) doped with ruthenium has a resistivity of 1 x 10^{-5} Ωm [3]. Both materials have a much higher resistivity when compared to gold and its alloys (for example Au-6.3% Pt has a resistivity of 7.17 x 10^{-8} Ωm) [1].

A carbon nanotube surface (CNT) has potential as a material for MEMS relay applications as a contact material. In [4], Au contacts with a substrate coated with tangled single walled carbon nanotubes were investigated. The author measured the resistivity of the SWCNT sheet to be

between 1 x 10^{-4} and 1.8 x 10^{-4} Ωm. Firstly, CNT-CNT pair was made in contact at a maximum load of 500mN and the average contact resistance is 0.87Ω. Secondly, an Au-CNT pair with contact load up to 150mN was performed and the contact resistance is ~2Ω. The authors concluded that a tangled SWNT film against an Au coated surface works better than two contacting tangled films but that a large force is needed to bend the CNT and obtain more contact points [4]. The following mechanical properties have been determined for CNTs; a tensile strength of 63 GPa (compared with 1.2 GPa for high strength steel) [5]. Experiments using atomic force microscopy have been performed to measure the elastic modulus and bending strength of individual structurally isolated multi-wall carbon nanotubes indicated values of 1.26 TPa and 14.2 GPa [6] respectively. Experiments have also been conducted on CNTs using nano-indentation apparatus and values were obtained for the bending modulus; 1.24 TPa, axial modulus; 1.23 TPa and wall modulus; 5.61 TPa [7]. Another report shows that CNT's have an elastic modulus greater than 1 TPa [8] compared to diamond, which is 1.2 TPa.

It is estimated that a 4-10 μm long Single Walled Carbon Nanotube (SWNT) with a diameter of 1.2nm has a resistivity of 0.88 x 10^{-8} Ωm [9] and is thought to exhibit ballistic electrical conduction. In addition, when a CNT is filled with metal, to form a composite, the resistivity falls to 0.35 x 10^{-8} Ωm [9]. The mechanical and electrical properties are therefore potentially comparable to diamond and gold respectively. No experiments have been reported on CNT materials for micro-contact applications. The study presented here investigates the application of a CNT metal matrix surface as a potential electrical contact material for low force applications.

II. MATERIAL PREPARATION AND EXPERIMENTAL METHODS

In this study three contact pairs have been investigated; Sample 1: Au to Au, Sample 2: Au to multi walled carbon nano-tubes (MWNT) and Sample 3: Au to Au/MWNT composite. The geometry selected is shown in Fig.1 with a 2mm diameter hemisphere contacting a flat surface. In all cases the hemisphere consists of a stainless steel base, sputter coated with Au, 500 nm thick, with surface roughness $R_a \approx 400$nm.

In experiment 1, the flat surface is a silicon (Si) substrate (~5mm by ~5mm), sputter coated with Au 500 nm, with a surface roughness $R_a \approx 30$nm. In experiment 2, a "forest" of MWNT is grown on the Si wafer as shown in Fig 2 using thermal CVD. The catalyst used is sputter deposited Fe and

the gaseous carbon source is ethylene. The growth temperature and time is 875^{o}C and 3 minutes respectively to produce vertically aligned MWNT of ~50μm in length. Experiment 3 is the same as experiment 2, but with Au sputtered on the upper surface of the MWNT forest (50μm in length) to produce Au/MWNT composite coatings as shown in Fig 3. It is shown that the Au penetrates the MWNT surface to a depth of 2 to 4 μm.

To achieve the low forces (<1mN) with a high degree of repeatability a modified nano-indentation apparatus [10] is used. The diamond indenter tip is replaced with the hemispherical contact surfaces shown in Fig's 4 and 5. The force and electrical contact resistance (CR) can be measured simultaneously. The force measurement is intrinsic to the apparatus and the CR is measured using the 4-wire measurement method as shown Fig 5. The DC current source across the micro-contact and the substrate is set at 1mA using a Keithley 580 micro-ohmmeter.

The experimental apparatus is maintained at a constant temperature of 31^{o}C. This is to prevent any thermal drift affecting the experiment due to expansion of the apparatus or the specimens. The coated micro-contact and substrate are brought into contact at a controlled loading rate of 0.2 mN/s until the maximum load of 1 mN is reached. The targeted load is held for 10 seconds so that an average peak load resistance value can be determined. The contacts are unloaded at the same rate until they are separated. Fig 6 shows an example of the CR variation over one load cycle. Over the first 5 seconds as the contact are loaded the contact resistance falls and then remains relatively stable during the holding time; during the unloading period the contacts remain together after 20 s, which is a result of the Au contacts "sticking". The procedure is repeated in order to detect any cyclic changes in the electrical contact resistance.

Prior to the experiments, two control measures are used. (1); To determine the bulk resistance of the component. By changing the width between the Sense (-ve) and Source(-ve) point on the substrate, Fig 7. In addition the micro-contact position is moved relative to the current source connections, at 100nm and 200nm as shown schematically in Fig 7. Both tests result in the same resistance reading ~0.38Ω. This confirms that the 4-wire measurement method is a measure of the contact resistance and not the bulk resistance. (2) To determine the nature of the film conduction. In this test the contact resistance across the Au micro-contact with the substrate coated by the catalyst only (i.e. no MWNT) is measured and no conduction is detected. This shows that the electrical conduction mechanism is through the MWNT and Au/MWNT coatings. This

observation is expected to have important implications in the evaluation of the contact resistance [11].

III. RESULTS AND DISCUSSION.

A. Load-contact resistance characteristic for experiment 1 (Au-Au)

Fig 8 shows the experimental contact resistance versus contact force characteristic of the Au-Au contact pair up to a maximum load of 1mN. At very low forces below 0.1mN the average contact resistance during the holding period is approximately 0.5Ω, which decreases to 0.4Ω at 1mN. The figure also shows the contact resistance based on theoretical predictions. Assuming that the contact deforms plastically, based on the Holm analytical model, [12], using the following equation:

$$R_c = \left(\frac{\rho^2 \eta \pi H}{4F} \right)^{\frac{1}{2}} \qquad \textit{(eqn. 1)}$$

Where for Au: $\rho = 2.24 \times 10^{-8}$ Ωm.

and for sputtered Au. [13]: $H = 1.7 \times 10^{9}$ N/m^2,

The measured contact resistance data are significantly greater than the analytical model using the above formula. There are three possible reasons for this difference:

(i) In the analytical model the contact surfaces are assumed to be clean (assume η=1) but in the experiment there are likely to be surface films and contaminants thus giving a higher contact resistance.

(ii) the classical Holm model assumes an electron diffusion dominated conduction model. Under low force conditions the model requires modification. [13, 22].

(iii) the classical Holm model assumes an infinitely large conducting body, the model will be compromised by the thin film conduction mechanism. Both the substrate and the ball are coated in 0.5μm Au films. The bulk materials are non-conducting for the substrate and also likely to be non-conducting for the stainless steel ball.

B. Consideration of the Au Film Contamination.

Gold is a logical choice as contact material for MEMS relay applications because it has a low propensity to form alien surface films, and is corrosion resistant [13]. However, Au has the tendency to have a thin layer of adventitious carbon on its surface that is residue from the cleaning process and/or is adsorbed due to exposure to air [14]. For example, it has been reported that there are 2-4 nm thick of adsorbed hydrocarbons on freshly cleaned Au [15,16] and this will increase the contact resistance. Therefore, surface films and contaminants should not be ignored when designing a new contact resistance analytical model. In addition, the use of a single effective contact area rather than multiple a-spots should be reconsidered. At low contact force, multiple a-spot's will be formed during contact because of the asperities on the surface. The asperities will have different height and radius [12]. The investigation of the influence of the position of the resistance sensing probes on the resistance measurement suggests that any influence from contamination would be expected to be uniform over the surface. It is thus proposed that the contamination is negligible and that the assumption that $\eta=1$, is valid.

C. Modification of the Holm model for low force contacts.

Consideration is firstly given to the breakdown of the classical Holm conduction model. This follows a study by Coutu et.al., where the influence of elastic-plastic material deformation and the associated contact resistance under the low force conditions typical of MEMS relays, where conduction is likely to be dominated by ballistic and diffusive electron transport; were considered [13]. Using the formula from [13];

$$R'_c = R_c\,(ballistic) + \Gamma(K) R_c\,(diffusive) \qquad (eqn.\ 2)$$

Where R_c *(ballistic)* is the contact resistance equation based on ballistic electron transport and elastic-plastic material deformation, R_c *(diffusive)* is the contact resistance equation based on diffusive electron transport and elastic-plastic material deformation and $\Gamma(K)$ is the Gamma function. This formulation is an updated micro-contact resistance model for low force contact developed using Chang's [17] improvement to the Chang, Etsion, and Bogy (CEB) model [18] and the Gamma function in Wexler interpolation [19]. Where;

$$R_c(ballistic\ ) = \frac{4\rho K}{3\pi}\sqrt{\frac{H\pi\left[1.062\ + 0.354\left(\frac{2}{3}K_Y - 3\left(\frac{\alpha_c}{\alpha}\right)\right)\right]}{F}} \qquad (eqn.\ 3)$$

R_c(ballistic) is the contact resistance equation based on ballistic electron transport and elastic-plastic material deformation, ρ is the resistivity of sputtered Au on the micro-contact, H is the hardness of sputtered Au, F is the applied load (range from 10μN to 1mN), K is Knudsen number, K_Y is the yield coefficient, α_c is the critical vertical deformation, α is the asperity vertical deformation.

$$R_c(diffusive\ ) = \frac{\rho}{2}\sqrt{\frac{H\pi\left[1.062 + 0.354\left(\frac{2}{3}K_Y - 3\left(\frac{\alpha_c}{\alpha}\right)\right)\right]}{F}} \qquad (eqn.\ 4)$$

R_c(diffusive) is the contact resistance equation based on diffusive electron transport and elastic-plastic material deformation. To calculate the Knudsen number [13,20];

$$K = \frac{l_e}{r_{eff}} \qquad (eqn.\ 5)$$

The Knudsen number, K, is a dimensionless number describing the flow of the electron particles and is defined as the ratio of the molecular mean free path length to a representative physical length scale; the length scale example would be the radius of the contact surface. l_e is elastic mean path (for most metals ~50 nm [13,20]) and r_{eff} is effective contact area radius. In a single effective asperity model, the individual contact spots are close enough together that their interactions are not independent. In this circumstance [13] assumes that the effective contact area is defined as the sum and not the parallel combination of the individual contact areas.

To understand the implication of the modified contact resistance model consider the 1mN contact force with the values of H and ρ used in eqn. 1, assume η=1, this leads to a predicted contact area of 0.58μm^2 based on A= F/H. This generates a predicted constriction resistance of 26mΩ as shown in Fig.8. The corresponding contact radius is 430nm, based on a single circular contact. The corresponding relationship with force is shown in Fig.8. As reported this shows a significant difference with the measured values. To determine the adjustment to the predicted resistance based

on the application of eqn's 2,3 and 4. If we assume the same area of contact then; using eqn. 5, K= 0.000116. Thus for the selected area the contribution to the resistance of the ballistic transmission model is negligible. To determine the contribution to the resistance resulting from the modified diffusive model; the yield coefficient can be calculated using [13];

$$K_Y = 1.1282 + 1.158v \qquad \textit{(eqn. 6)}$$

Where v is Poisson's ratio for Au (0.42), thus, K_Y is 1.61456. When the asperities are considered having elastic-plastic deformation, the α (asperity vertical deformation) and α_c (critical vertical deformation) are assumed equal [17,18]. To estimate the $\Gamma(K)$ Gamma function we can use the graph as shown in Fig. 9 [19,21,22]. Since K (Knudsen number) is 0.000116, from the graph the Gamma function is ~1. By substituting eqns. 3 and 4 and the above data into eqn. 2 a new analytical model is plotted as shown in Fig 8.

The new analytical model (eqn.2) gives a contact resistance slightly lower than Holm's contact resistance model in (eqn 1). In this model; (1) the new micro-contact resistance considers elastic-plastic material deformation, (2) it uses a single effective contact area rather than multiple a-spots, (3) conduction during the micro-relay's closure is considered to be a mixture of ballistic and diffusive electron transport, and (4) the contact load discontinuity (which exists at the transition from ideal elastic to ideal elastic-plastic behavior) is accounted for. The model falls short of the measured values and it is therefore concluded that the existing models for contact resistance are not applicable and further consideration should be given to the influence of thin film conduction.

D .Modified Contact Resistance for Thin-Films

The theory presented in the previous section is based upon the analysis of bulk materials. There are two additional factors not considered; the conduction in a thin film upon a non-conducting surface, and the local hardness value, which is expected to differ from the bulk value.

When the radius of the contact area is no longer small compared to the film thickness, the contact resistance is no longer dominated by the Holm constriction resistance, [22]. In this case a spreading resistance is required from the contact area to the thin metallic film. In the current study the radius of the contact area was estimated to be 430nm, which is comparable with the film thickness of 500nm. In the study an FEM model was used to show an increase in the constriction

resistance from 1mΩ using a modified version of the Holm equation, to 12mΩ using the FEM model, for a 1µm film, with a 5µm contact radius.

In this study an FEA model was created with a 500nm Au film, shown in Fig. 10, modelled on the 1mN contact force with the same values of H and ρ used in Eqn. 1. The model is a simple 2D axi-symmetric system, which models a 3D system with the current fed through a cylindrical electrode. This generates a predicted constriction resistance of 62mΩ, compared to the 26mΩ in Fig.8. The result from the FEM study identifies the importance of thin film conduction mechanisms, as being the most likely contribution to the increase in the measured values of resistance over the predicted values.

E. Load-contact resistance characteristic for experiment 2 (Au-MWNT)

Fig 11 shows the contact resistance against an applied load of the Au-MWNT contact pair. Fig 12 shows a scanned image of a MWNT surface showing asperities and a surface roughness, $R_a \approx 1.3\mu m$. Fig 13 shows a corresponding SEM image of the top surface of a MWNT coated surface. In this experiment, the dominant factor is expected to be the elastic deflection of the MWNTs rather than plastic indentation. As the applied load is increased, more deflection occurs of the MWNTs closing the air gaps between the vertically aligned MWNTs thus improving the transfer of electrons. Furthermore the MWNTs will conform to the form of the Au micro-contact, increasing the contact area.

F. Load-contact resistance characteristic for experiment 3 (Au-Au/MWNT)

In this case the contact resistance is lower than for the Au-MWNT contact pair and higher than Au-Au contact pair as shown in Fig. 14. The Au coating on MWNT makes contact with the Au coated ball thus leading to a decrease in the contact resistance.

G. Cyclic loading

To determine the performance of these materials under cyclic loading conditions, an initial study is presented using the nanoindenter apparatus to cycle for 10 repeated operations. Fig 15 shows the contact resistance of an Au-Au pair over 10 load cycles at a maximum applied load of 1mN. The

points include the corresponding standard deviation of the contact resistance measured during the hold period. A recent experiment [10] using a modified nano-indentation apparatus shows the Au-Pt contact pair degrading and the contact resistance increases after the 10^{th} cycle. It was proposed that this is due to hot-switched contact arcing.

In this experiment no current loading occurs so the contacts are unlikely to degrade by "hot-switching", therefore the increase in contact resistance is solely due to the deterioration of the Au-Au contact pair surfaces. Au is a very soft metal, typically with low hardness 1-2GPa [13], has a low melting point, and is susceptible to wear. Fig 16 shows the contact resistance of an Au-MWNT contact pair during cyclic load. The contact resistance of the Au-MWNT contact pair during cyclic load is much higher (~108 Ω) than the Au-Au contact pair (~0.39 Ω). Fig 15 also shows the contact resistance of an Au-Au/MWNT contact pair. The contact resistance is similar in pattern, where it shows stability over the first 10 loading cycles to the Au-MWNT contact pair (Fig 16) but lower (~0.46Ω).

H. Load-Displacement Characteristic of the surfaces

To investigate the performance of the materials details of the load displacement characteristics are used. Fig 17 shows a graph of indentation load versus displacement (data extracted from the nano-indentation apparatus). However, before describing them, we first describe the general features of the load-displacement responses we have observed from the experiment. The curve in region 1 shows the loading and the curve in region 3 shows the unloading of the micro-contact. The curve in region 2 shows there is creep, a deformation that occurs over a period of time when a material is subjected to constant stress, which may also be temperature-dependent. Region 4 is the permanent depth deformation after the contact pair separates. From Fig 17 it can be seen that the displacement of the Au-Au/MWNT contact pair is greater than for the Au-Au contact pair, this will provide a larger conducting surface area.

Fig 18 shows the comparison of Au-Au/MWNT with an Au-MWNT contact pair where the Au-Au/MWNT contact pair has a significant permanent indentation (Fig 18, at region '5') and the Au-MWNT contact pair shows much less permanent indentation (Fig 18 at region '6'). This is consistent with the MWNT deforming elastically whereas the Au undergoes plastic deformation. Fig 19, shows an SEM image of the Au (ball) contact surface after the load cycles. It shows some

damage to the Au surfaces. When an area marked 'A' was scanned using a non-contact 3D laser profiler (TaiCaan Xyris 4000CL) many small impressions on the Au micro-contact are detected as shown in a 3D scanned surface in Fig 20 (b), which can be compared to a new surface in Fig 20 (a). These impressions are due to the asperities on the MWNT surfaces. Moreover the surface roughness, R_a in this region has changed from ~400 nm to ~1.5μm.

Fig 19 shows the area analysed by X-ray spectroscopy on the Au (ball) micro-contact "Spectrum 1". Fig 21 shows an EDX spectrum for the surface. Gold is the predominantly observed element with carbon and oxygen also observed. This is consistent with the composition of the film, with some additional surface contamination and water adsorbtion. The overall atomic percent of Au is 38.60%, C is 55.49% and O 5.91% for the area "Spectrum 1". When a point on the exposed hemisphere (Au ball contact) was analysed, marked 'Spectrum 2', Fig 19. The 'Fe' peak was predominantly observed and Cr peak indicates both elements come from the stainless steel ball, Fig 22. The atomic percent shows Fe is 68.69%, Cr is 19.08%, C is 11.67% and Au is 0.57% thus indicating that wear has occurred on the Au micro-contact exposing the surface of the ball. No evidence of deformation or change in chemical composition on Au/MWNT surfaces can be detected.

Even though the Au-Au/MWNT contact pair shows improvement to the contact resistance, further development is needed, to avoid adhesion between the contact pair, which could degrade the contact resistance during extended load cycles. This phenomenon is clearly seen in Fig 6 where during unloading there is still contact resistance measured until total separation of the contact pair. Moreover, creep can be seen in Fig 17 (curve at region 2) this is identified as the mechanism responsible for the increase in stiction [23]. A fundamental understanding of the relationships between contact force, adhesion, and contact resistance is needed for MEMS relay design [24].

IV. CONCLUSION.

The contact force and contact resistance between Au-Au/MWNT composite contact pairs was investigated using a modified nano-indentation apparatus and 4-wire measurement methods. The contact pair combination was compared to a Au-MWNT pair, and showed a decrease in the measured contact resistance. The performance of the Au-Au/MWNT composite contact pairs was comparable to an Au-Au contact pair also studied as a benchmark for the new material.

Furthermore during ten load cycles, the Au-Au/MWNT contact pair showed stable and constant contact resistance.

A study of contact resistance modeling based on existing analytical models shows that there is a discrepancy with the benchmark Au-Au surface. This leads to the conclusion that the mechanics of such surfaces at low force must fall outside the current understanding. An initial study suggests that the main reason for the difference is due to the conduction mechanisms associated with thin film surfaces. An FEA analysis shows that conduction through the thin film conductor leads to an increase in the predicted resistance, but that further modifications to the model are required.

This experimental method is applicable to MEMS relay micro-contacts and will serve as a platform for our future research and investigations of Au/MWNT-Au/MWNT and Au/SWNT-Au/SWNT contact pairs with different packing densities and length of CNT and thickness of the Au coatings on the carbon nanotubes.

Acknowledgements

The authors would like to thank Dr. S.Abu-Sharkh of the School of Engineering Sciences for his contribution to the FEA study, and to Dr D.C. Smith of the School of Physics and Astronomy, for providing the facilities for depositing the MWNT and Au.

References

[1] Coutu, R. A., Kladitis, P. E., Leedy, K. D. and Crane, R. L., 2004, "*Selecting Metal Alloy Electric Contact Materials for MEMS Switches*," Journal of Micromechanics and Microengineering, (14) pp. 1157-1164.

[2] Gao, D., Wijesundara, M. B. J., Carraro, C., Low, C. W., Howe, R. T. and Maboudian, R., 2003, "*High Modulus Polycrystalline 3C-SiC Technology for RF MEMS*," The 12th International Conference on Solid State Sensors, Actuators and Mircosystems, 3D3.4, pp. 1160-1163.

[3] Lian, G. D., Dickey, E. C., Ueno, M. and Sunkara, M. K., 2002, "*Ru-doped Nanostructured Carbon Films*," Diamond and Related Materials, 11, pp. 1890-1896.

[4] Yaglioglu, O., Hart, A. J., Martens, R. and Slocum, A. H., 2006, *"Method of characterizing electrical contact properties of carbon nanotube coated surfaces,"* Review of Scientific Instruments, 77, pp 095105/1-3.

[5] Yu, M. F., Lourie, O., Dyer, M. J., Moloni, K., Kelly, T. F. and Ruoff, R.S., 2000, "*Strength and Breaking Mechanism of Multiwalled Carbon Nanotubes Under Tensile Load*," Science, 287(5453), pp. 637 – 640.

[6] Wong EW, Sheehan PE, Lieber CM, 1997 "*Nanobeam Mechanics: Elasticity, Strength, and Toughness of Nanorods and Nanotubes*," Science, 277, pp. 1971-5.

[7] Qi, H.J., Teo, K.B.K., Lau, K.K.S., Boyce, M.C., Milne, W.I., Robertson, J. and Gleason, K.K., 2003, "*Determination of Mechanical Properties of Carbon Nanotubes and Vertically*

Aligned Carbon Nanotube forests using Nanoindentation," Journal of Mechanics and Physics of Solids, 51, pp. 2213-2237.
[8] Thostenson, E. T., Ren, Z. and Chou, T.W., 2001, "*Advances in the Science and Technology of Carbon Nanotubes and their Composites: A review,*" Composites Science and Technology, 61, pp. 1899-1912.
[9] Hjortstam, O., Isberg, P., Söderholm, S. and Dai, H., 2004, *"Can we achieve ultra-low resistivity in carbon nanotube-based metal composites?"* Journal of Applied Physics A, Materials Science & Processing, 78, pp. 1175-1179.
[10] Dickrell III, D. J. and Dugger, M. T., 2005, "*The effects of surface contamination on resistance degradation of hot-switched low-force MEMS electrical contacts*," Electrical Contacts, Proceedings of the Annual Holm Conference on Electrical Contacts, v 2005, Electrical Contacts 2005 - Proceedings of the Fifty-First IEEE Holm Conference on Electrical Contacts, pp. 255-258.
[11] Norberg, G., Dejanovic, S., and Hesselbom, H., 2006, *"Contact Resistance of Thin Metal Film Contacts,"* IEEE Transactions on Component and Packaging Technologies, v.29, n.2, pp. 371-378.
[12] McBride, J. W. 2006, *"The Loaded Surface Profile: A new technique for the investigation of contact surfaces,"* International Conference on Electrical Contacts 2006, pp. 150-156.
[13] Coutu, R.A., Jr., Reid, J.R., Cortez, R., Strawser, R.E., and Kladitis, P.E., 2006, "*Microswitches with sputtered Au, AuPd,Au-on-AuPt, and AuPtCu alloy electric contacts*," IEEE Transactions on Components and Packaging Technologies, v 29, n 2, pp. 341-9.
[14] Patton, S.T., Zabinski, J.S., 2005, *"Fundamental studies of Au contacts in MEMS RF switches,"* Tribology Letters, v18, n 2, pp. 215-230.
[15] Hyman, D. and Mehregany, M., 1999, *"Contact physics of gold microcontacts for MEMS switches,"* IEEE Transactions on Components and Packaging Technologies, v 22, pp.357-64.
[16] Tringe, J., Wilson, W.G., and Houston, J.E., 2001, *"Conduction properties of microscopic gold contact surfaces Source,"* Proceedings of the SPIE - The International Society for Optical Engineering, v 4558, pp. 151-8.
[17] Chang. W., 1997, "*An elastic-plastic model for a rough surface with an ion-plated metallic coating*," Journal of Wear, v.212, pp. 229-237.
[18] Chang, W.R., Etsion, I. and Bogy, D.B., 1987, "*An elastic-plastic model for the contact of rough surfaces*," Transactions of the ASME. Journal of Tribology, v 109, n 2, pp. 257-63.
[19] Mikrajuddin, A., Shi, F.G., Kim, H.K. and Okuyama, K., 1999, "*Size-dependent electrical constriction resistance for contacts of arbitrary size: from Sharvin to Holm limits*," Materials Science in Semiconductor Processing, v 2, n 4, pp. 321-7.
[20] Agrait, N., Yeyati, A.L. and van Ruitenbeek, J.M., 2003, *"Quantum properties of atomic-sized conductors,"* Physics Reports, v 377, n 2-3, pp. 81-279.
[21] Wexler, G., 1966, "*The size effect and the nonlocal Boltzmann transport equation in orifice and disk geometry*," in Proceedings of the Physical Society, v 89, pp. 927-941.
[22] Timsit, R.S., 2006, *"Electrical Conduction Through Small Contact Spots*," IEEE Transactions on Components and Packaging Technologies, v.29, n 4, pp. 727-734
[23] Gregori, G. and Clarke, D. R., 2006, "*The interrelation between adhesion, contact creep, and roughness on the life of gold contacts in radio-frequency microswitches,*" Journal of Applied Physics, 100, pp.094904-1/10.
[24] Schimkat, J. 1999, *"Contact measurements providing basic design data for microrelay actuators,"* Sensors and Actuators A (Physical), v A73, n 1-2, pp. 138-43.

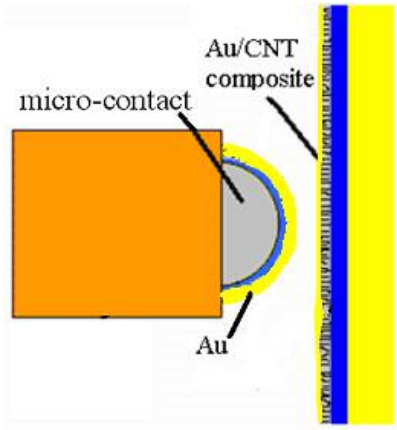

Figure 1: Schematic layout of the Au-Micro-contact and Au/CNT composite Substrate.

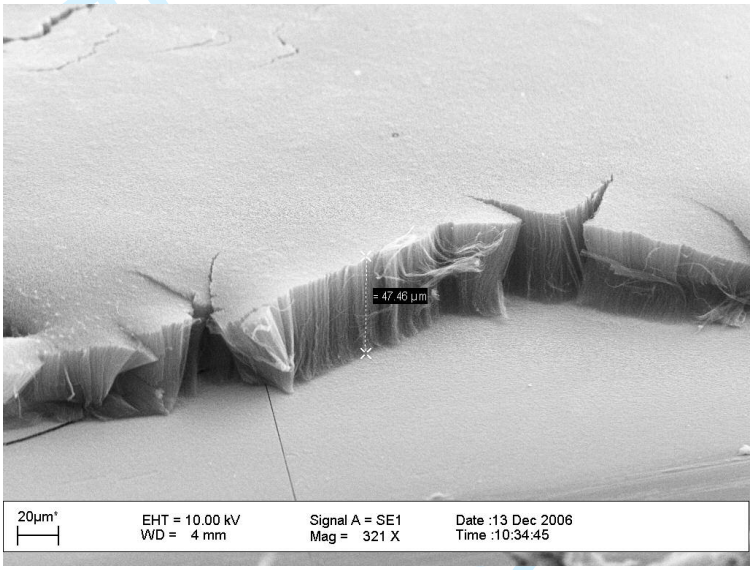

Figure 2: Sample 2, SEM image of a forest of MWNTs on an Si substrate.

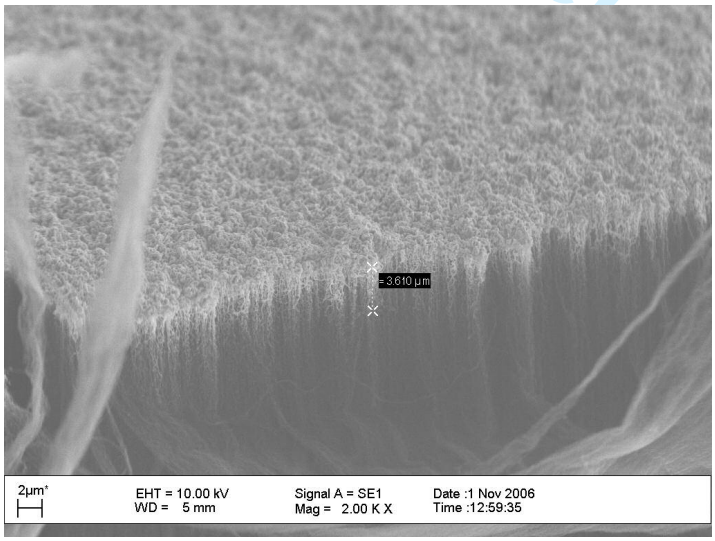

Figure 3: Sample 3, 2 - 4µm of Au coating on MWNT by sputtering.

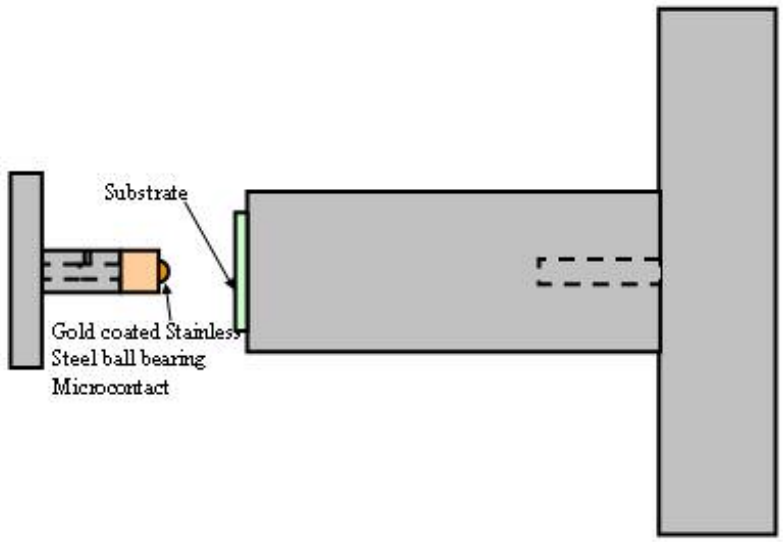

Figure 4: Schematic of modified nanoindenter.

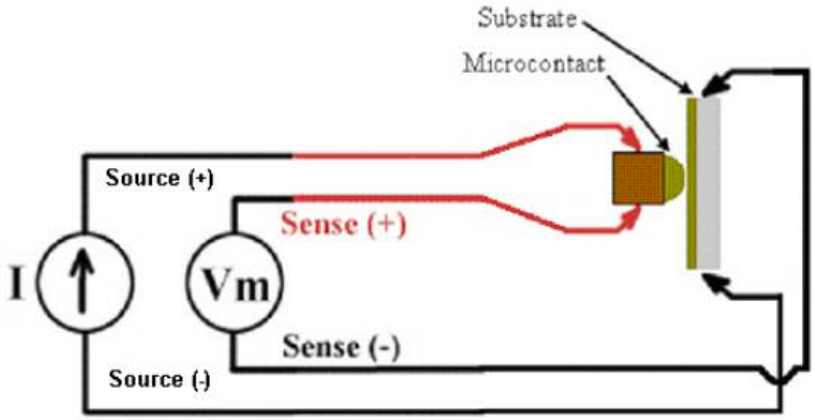

Figure 5: Schematic of contact zone with its electrode and R_c measurement.

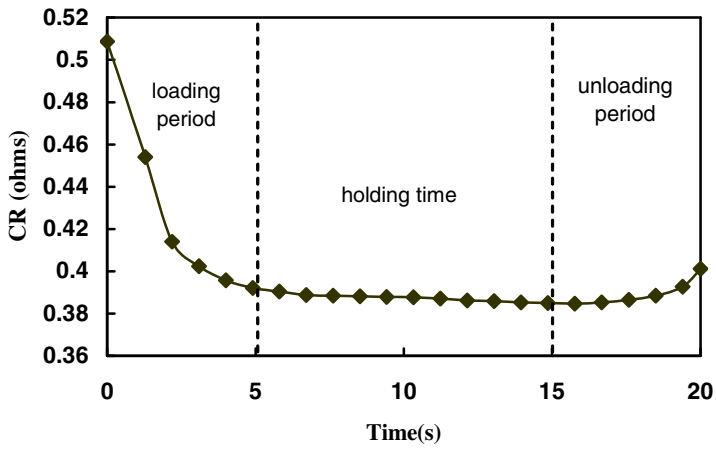

Figure 6: Example of one load cycle for an Au-Au contact pair.

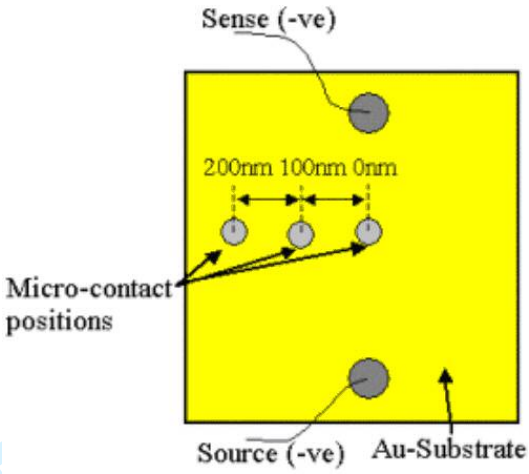

Figure 7: Top view micro-contact positions on the Au-substrate.

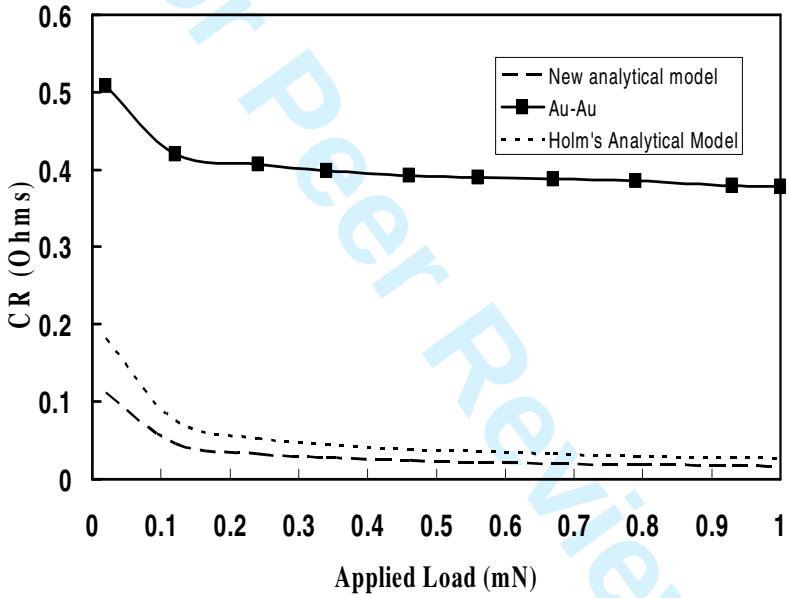

Figure 8: Contact resistance between Au-Au contact pair as a function of the applied load.

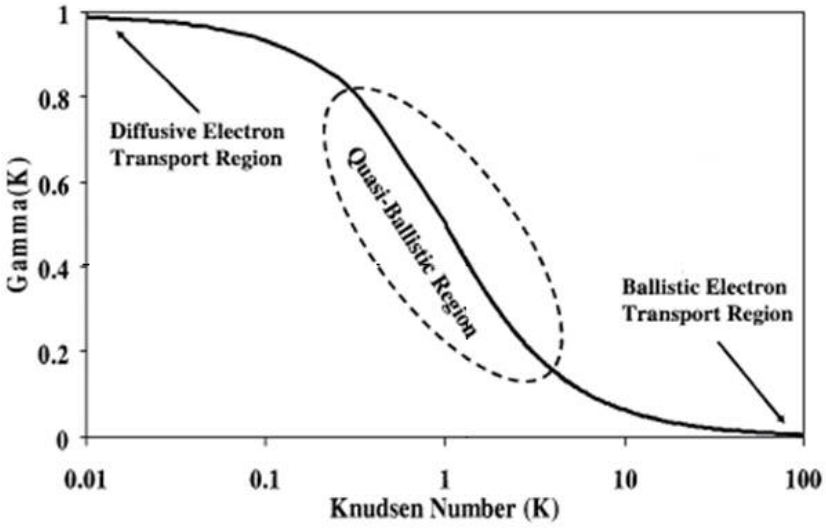

Figure 9: Plot of Mikrajuddin et.al.'s derived gamma function.

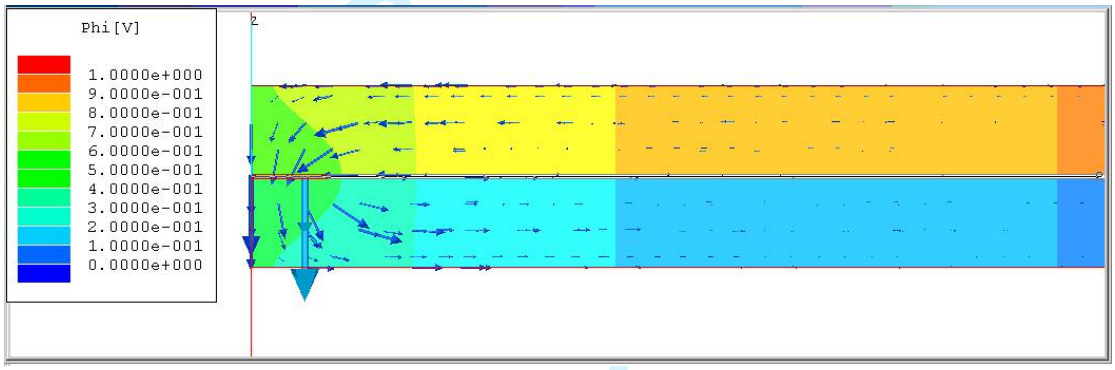

Figure 10: FEA model of thin film with current flow through a 500nm Au film with a contact area of 0.58μm^2.

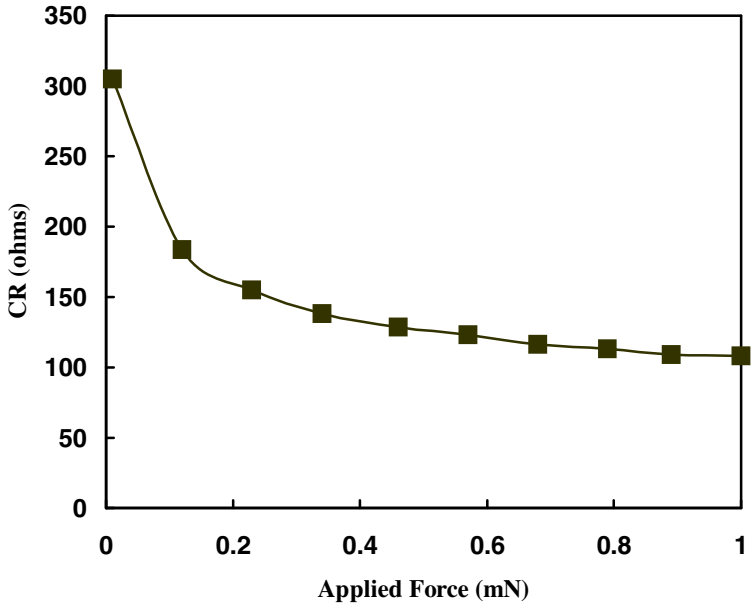

Figure 11: Contact resistance between Au-MWNT contact pair as a function of applied load.

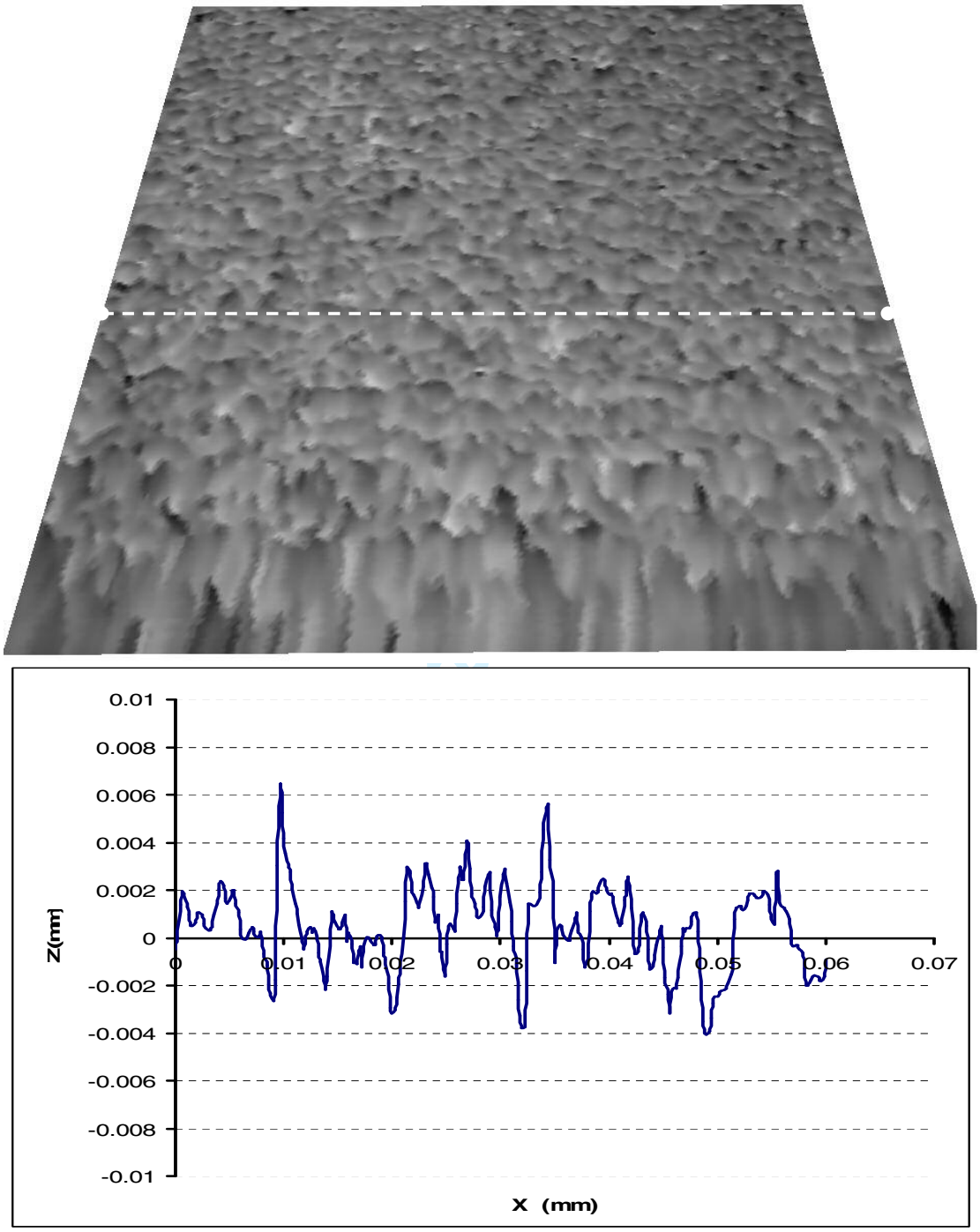

Figure 12: Con-focal Laser Scanned image of MWNT 301x301 (60µm x 60µm) using TaiCaan Technologies (Xyris 4000CL), showing 2D section of data.

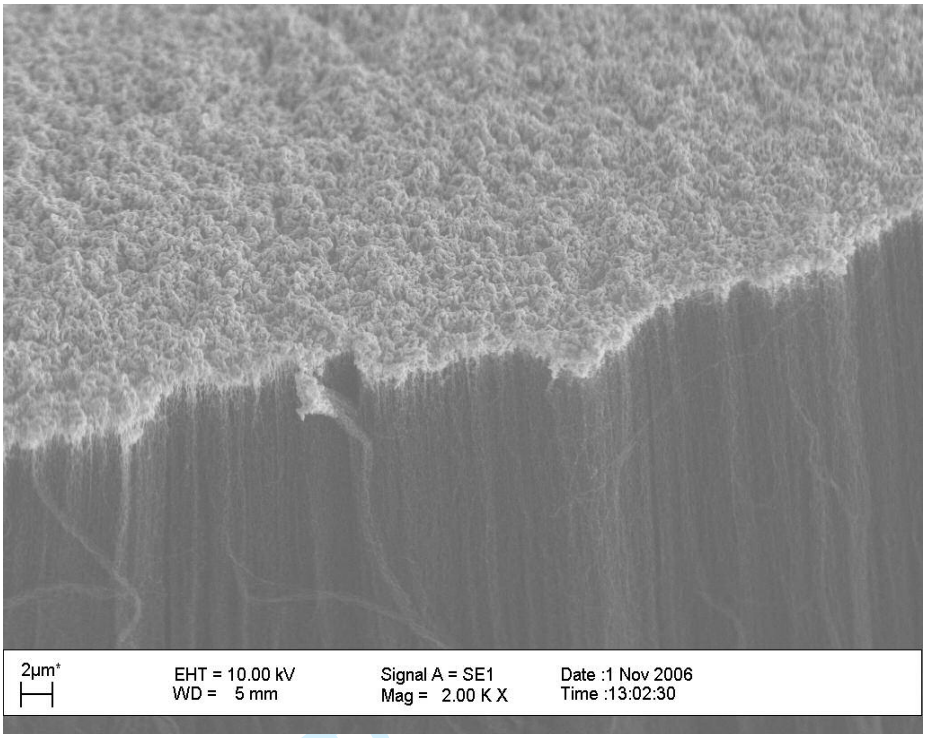

Figure 13: SEM image of MWNT with over-coating of Au.

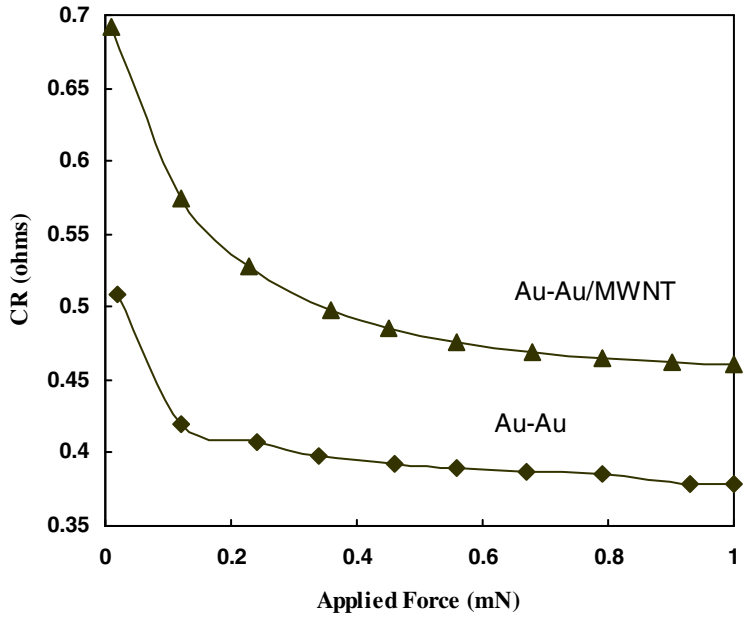

Figure 14: Contact resistance between Au-Au and Au-Au/MWNT coating contact pair as a function of applied load.

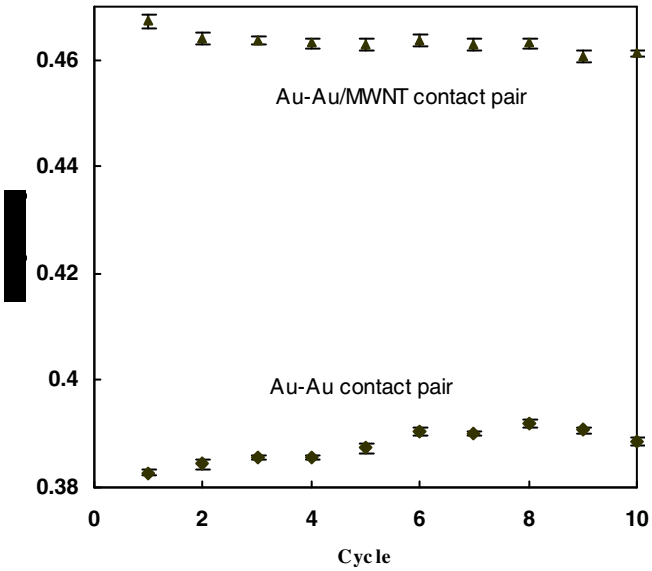

Figure 15: Cyclic contact resistance of Au-Au and Au-Au/MWNT contact pair.

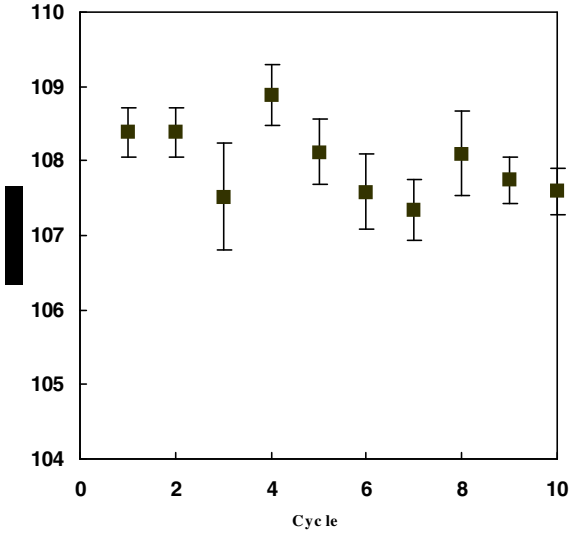

Figure 16: Cyclic contact resistance of an Au-MWNT contact pair.

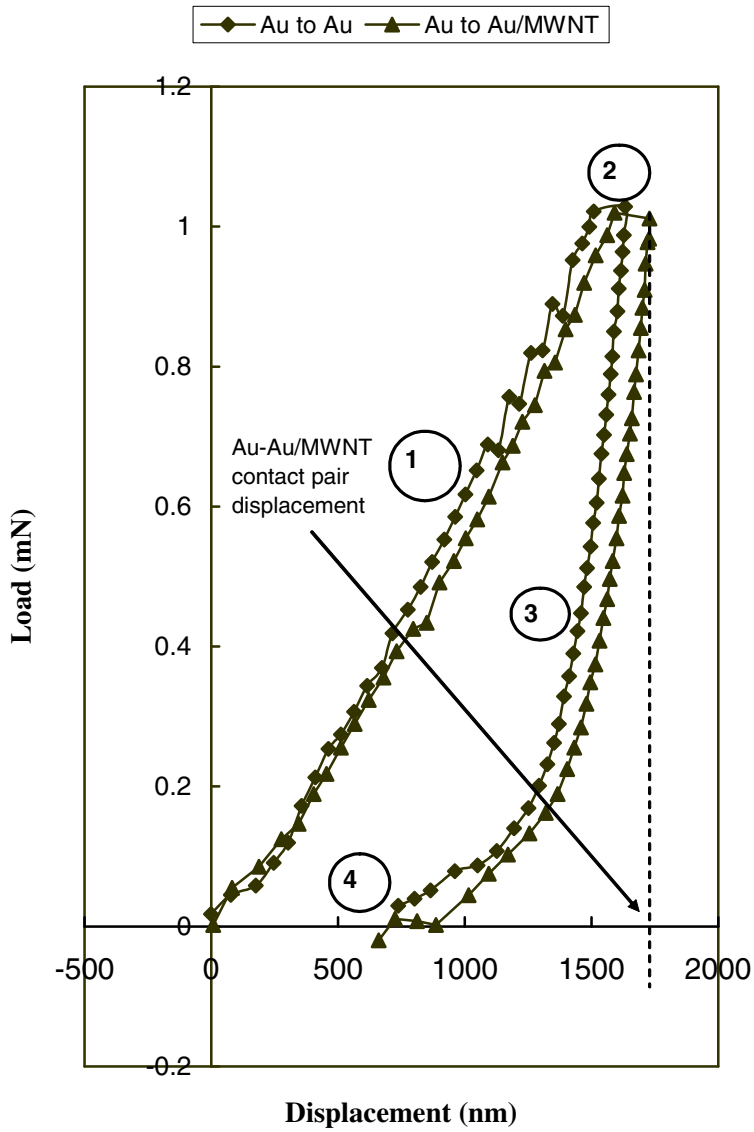

Figure 17: Graph of applied indentation load vs displacement (depth).

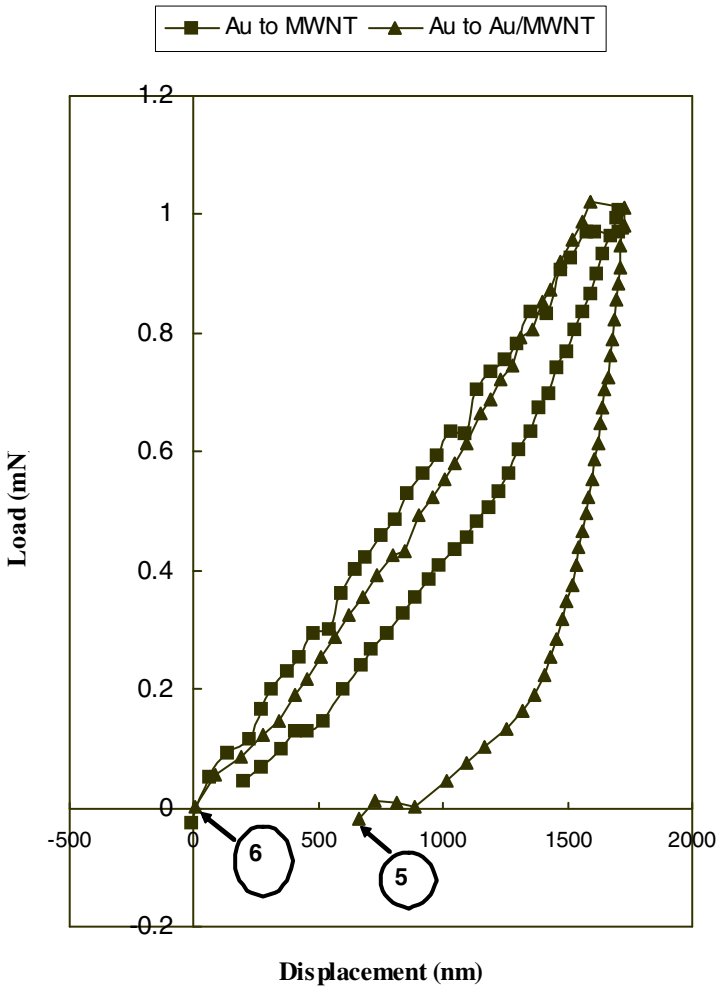

Figure 18: Graph of indentation load vs. displacement (depth) for Au-MWNT

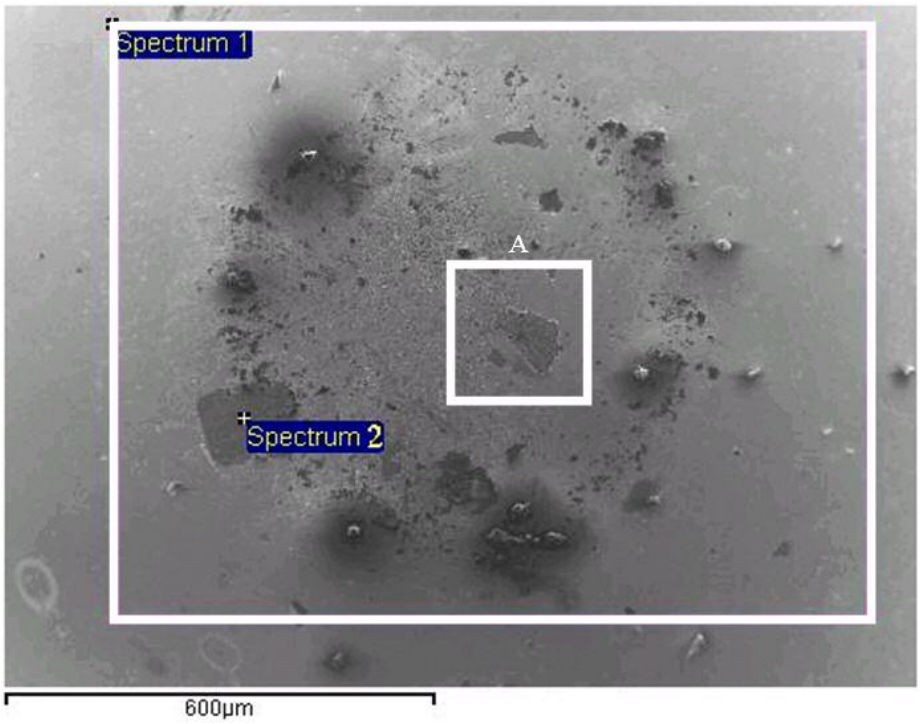

Figure 19: Au micro-contact after contact with Au/MWNT substrate.

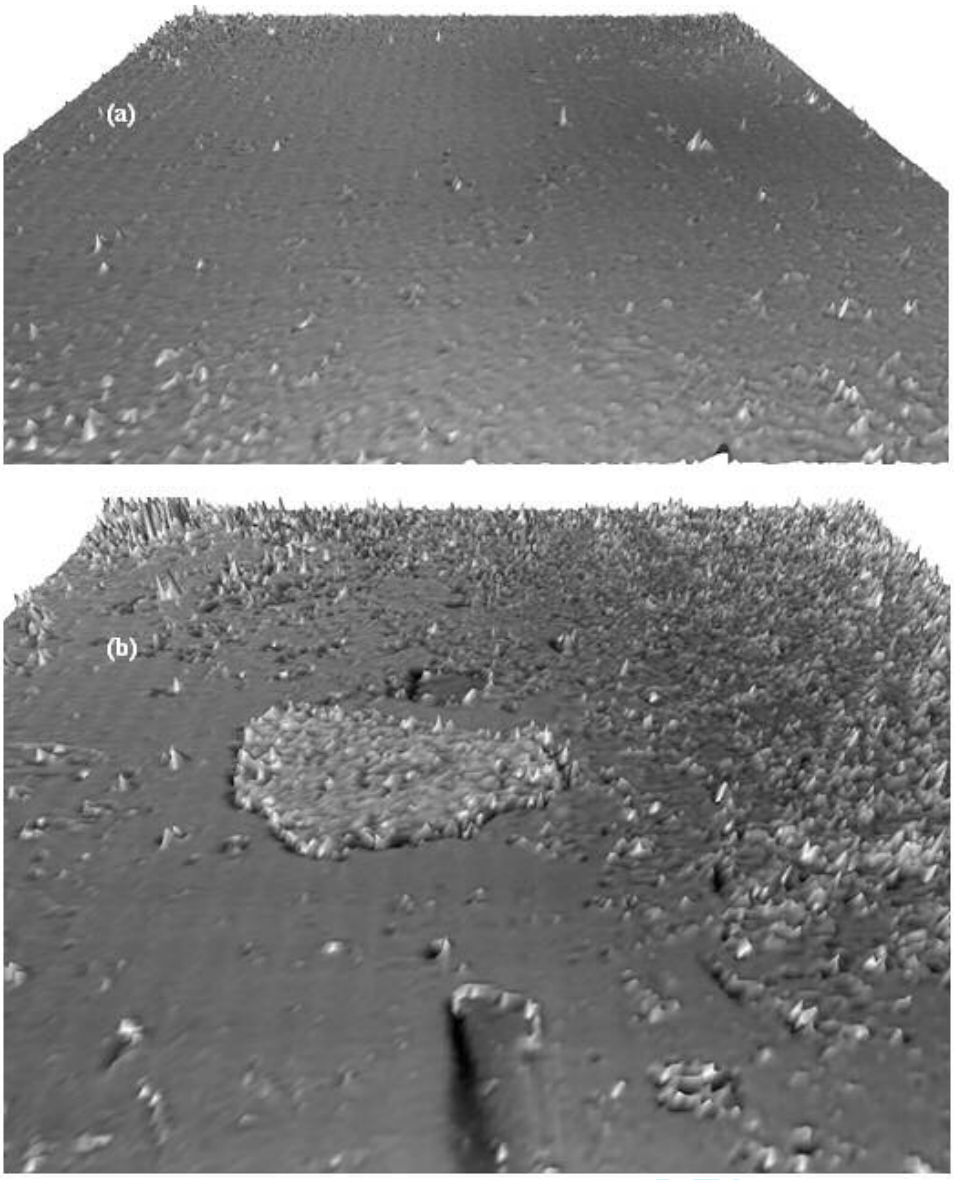

Figure 20: (a) Fresh and (b) tested Au (ball) micro-contact with spherical shape removed, 301x301 (400µm x 400µm) using TaiCaan (Xyris 4000CL).

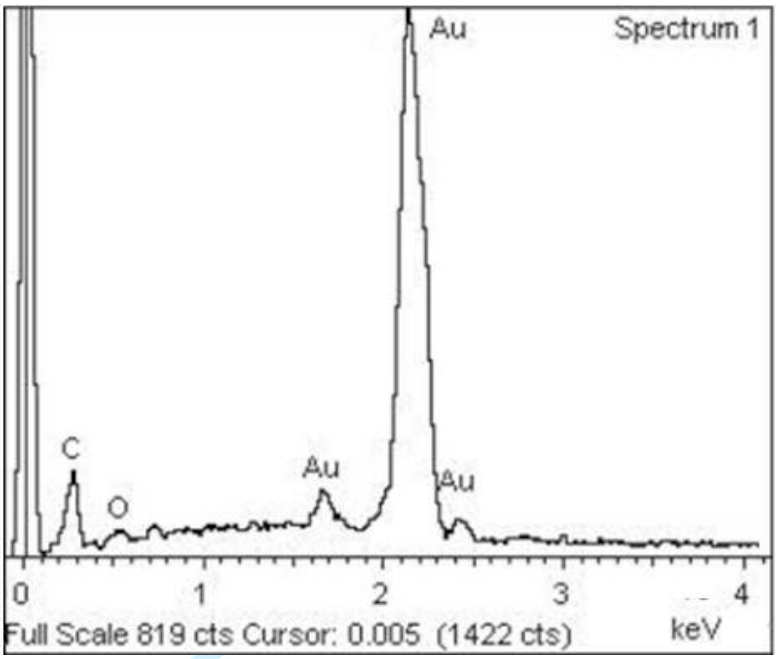

Figure 21: EDX spectrum of Au micro-contact surface.

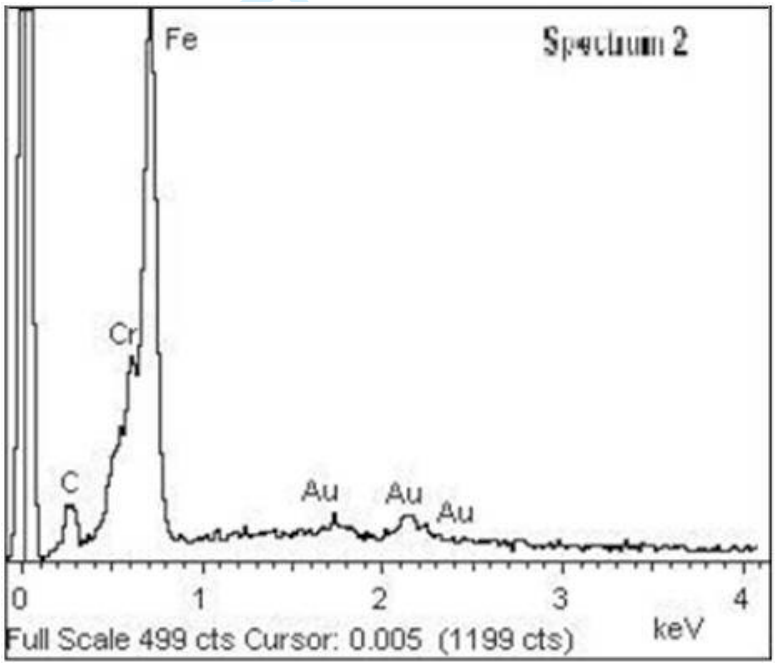

Figure 22: EDX spectrum of exposed hemisphere on the Au micro-contact surface.